RSC Advances

PAPER

View Article Online
View Journal | View Issue

Cite this: *RSC Adv.*, 2022, **12**, 31451

Ligand functionalization of defect-engineered Ni-MOF-74†

Jaewoong Lim, ‡ Seonghwan Lee,‡ Amitosh Sharma, Junmo Seong, Seung Bin Baek * and Myoung Soo Lah *

Incorporating functionality into the framework of metal–organic frameworks (MOFs) has attracted substantial interest because the physical and chemical properties of MOFs can be tuned by functionalizing pores. The ligand functionalization of MOF-74 is challenging because of its pristine organic ligand and framework structure. Herein, we report a series of ligand-functionalized Ni-MOF-74 derivatives synthesized by defect engineering using a mixed-ligand approach. Defect generation and ligand functionalization of Ni-MOF-74 were simultaneously achieved by incorporation of fragmented organic ligands such as 5-formylsalicylic acid, 3-hydroxysalicylic acid, 2-hydroxynicotinic acid and 5-hydroxy-1*H*-benzimidazole-4-carboxylic acid. The resulting defect-engineered Ni-MOF-74 derivatives maintained relatively good crystallinity up to fragment incorporation levels of ~20% and exhibited modified permanent porosity and CO_2 adsorption properties depending on the functional groups and defect concentrations in the framework.

Received 19th October 2022
Accepted 27th October 2022

DOI: 10.1039/d2ra06587h

rsc.li/rsc-advances

1. Introduction

The defect engineering of metal–organic frameworks (MOFs) has received increasing interest because MOFs with certain structural defects can outperform defect-free MOFs in many applications.[1–4] Among several reported defect generation methods, fragmented ligand installation has been confirmed to be a simple and efficient synthetic strategy to induce defects in MOF structures, where the fragment exhibits lower connectivity than the pristine ligand.[5–7] In general, fragmented ligand installation employs a mixed-ligand synthesis approach[8] that can efficiently introduce various functionalities into MOFs while retaining the parent MOF structure. Mixing the pristine ligand with its fragmented derivatives during synthesis can change the local coordination environments of the metal centers, which results in defect sites in the MOFs, thereby affecting their chemical and structural properties.

MOF-74 is an intensively explored MOF because of its high density of potential open metal sites, high porosity, and high surface area.[9,10] It features chains of metal ions linked by tetratopic 2,5-dioxido-1,4-benzenedicarboxylate ($DOBDC^{4-}$) to yield one-dimensional hexagonal channels. The defect engineering of MOF-74 has been relatively uninvestigated, presumably because of the difficulty in integrating fragmented ligands into an extremely rigid framework instead of the highly connected pristine ligand. Recently, a few reports on the defect engineering of MOF-74 using fragmented organic ligands have been published.[11–14] These reports revealed that structural defects in MOF-74 can be created only when 2-hydroxy-1,4-benzenedicarboxylic acid (H_2BDC-OH) is used as the fragmented ligand, suggesting that the coexistence of two –COOH and one –OH coordinating groups is a prerequisite for the defect formation of MOF-74. Recently, we established a *de novo* synthetic route to induce structural defects in Ni-MOF-74 using salicylic acid as a fragmented ligand with only one –COOH and one –OH as coordinating groups.[15] Furthermore, applying the same synthetic protocol, we demonstrated that 3- and 5-aminosalicylic acids could be incorporated into the Ni-MOF-74 framework, generating amine-tagged defect-engineered Ni-MOF-74 derivatives, the first examples of ligand-functionalized MOF-74 materials.[15]

The functionalization of defect-engineered MOFs has received little attention during the past decade, although the incorporated functionality may confer new promising properties to defect-engineered MOFs.[15–17] In this paper, we report the synthesis of a series of functionalized defect-engineered Ni-MOF-74 derivatives and their CO_2 adsorption properties. Aldehyde- and hydroxy-functionalized defect-engineered derivatives were prepared by direct solvothermal synthesis using a mixed-ligand approach with 5-formylsalicylic acid (H_2-5-fSA) and 3-hydroxysalicylic acid (H_2-3-hSA) as fragmented organic ligands (Fig. 1). We demonstrated that heteroaromatic fragments, 2-hydroxynicotinic acid (H_2-2-hNA) and 5-hydroxy-1*H*-benzimidazole-4-carboxylic acid (H_2-5-hBImCA) could also be

Department of Chemistry, Ulsan National Institute of Science and Technology (UNIST), 50 UNIST-gil, Ulsan 44919, Korea. E-mail: sbbaek@unist.ac.kr; mslah@unist.ac.kr

† Electronic supplementary information (ESI) available. See DOI: https://doi.org/10.1039/d2ra06587h

‡ These authors contributed equally to this work.

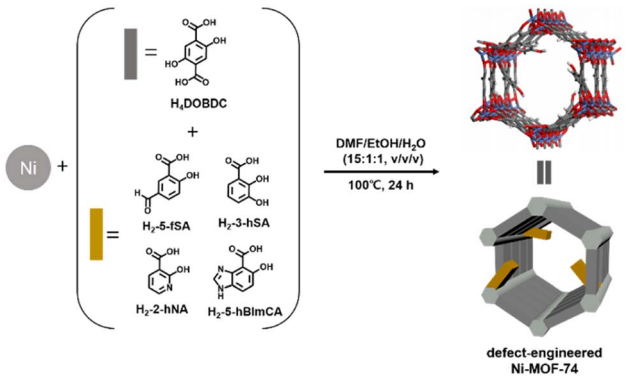

Fig. 1 Schematic representation of simultaneous defect generation and functionalization of Ni-MOF-74 by a mixed-ligand synthesis.

incorporated into the Ni-MOF-74 framework. The resulting Ni-MOF-74 derivatives maintained their crystallinity up to the fragment incorporation levels of ~20% and exhibited permanent porosity with surface areas of 640–1325 $m^2\ g^{-1}$. The CO_2 uptake strongly correlated more with the surface area than with the pore volume of the defect-engineered Ni-MOF-74 derivatives. The CO_2 uptake was affected by the type of incorporated functional group and by its position and size. The defect-engineered Ni-MOF-74 exhibited a lower isosteric heat of CO_2 adsorption compared with that of the pristine Ni-MOF-74, except for the 3-hydroxysalicylic acid-incorporated derivative.

2. Experimental

2.1. Synthesis of defect-free Ni-MOF-74

A solid mixture of $Ni(NO_3)_2 \cdot 6H_2O$ (198 mg, 0.680 mmol) and H_4DOBDC (95 mg, 0.480 mmol) was dissolved in 10 mL of a *N*,*N*-dimethylformamide (DMF)/ethanol (EtOH)/H_2O (15 : 1 : 1, v/v/v) mixed solvent. The solution was transferred to a 20 mL vial, tightly sealed and heated at 100 °C for 24 hours. The precipitate was collected, then washed three times using DMF, followed by solvent exchange with methanol (MeOH) over 3 days. The crystalline product kept stored in MeOH before use in the experiment.

2.2. Synthesis of defect-engineered Ni-MOF-74 derivatives

2.2.1. $[Ni_2(DOBDC)_{1-x}(5\text{-}fSA)_x(OH)_{2x}(H_2O)_{2+x}]$ (5-fSA$_x$). **5-fSA$_x$** was synthesized using a mixed ligand with 2,5-dihydroxy-1,4-benzenedicarboxylic acid (H_4DOBDC) and 5-formylsalicylic acid (H_2-5-fSA) at various mole ratios instead of pure H_4DOBDC. A solid mixture of $Ni(NO_3)_2 \cdot 6H_2O$ (198 mg, 0.680 mmol), 2,5-dihydroxy-1,4-benzenedicarboxylic acid (H_4DOBDC) (85.6 mg, 0.432 mmol) and H_2-5-fSA (8.0 mg, 0.048 mmol) was dissolved in 10 mL of a mixed solvent (15 : 1 : 1, DMF/EtOH/H_2O, v/v/v). The solution was transferred to a 20 mL vial, tightly sealed and heated at 100 °C for 24 hours, resulting in **5-fSA$_{0.08}$**. The precipitate was collected, then washed at least three times using DMF, followed by solvent exchange with MeOH for at least five times over 3 days. The same reactions with the mole ratio of H_4DOBDC : H_2-5-fSA at 7 : 3 and 5 : 5 produced **5-fSA$_{0.21}$**, and **5-fSA$_{0.39}$**, respectively. The crystalline product kept stored in MeOH before use in the experiment. The total amount of ligands used maintained 0.480 mmol for all the synthetic conditions.

2.2.2. $[Ni_2(DOBDC)_{1-x}(3\text{-}hSA)_x(OH)_{2x}(H_2O)_{2+x}]$ (3-hSA$_x$). A solid mixture of $Ni(NO_3)_2 \cdot 6H_2O$ (198 mg, 0.680 mmol), H_4DOBDC (85.6 mg, 0.432 mmol) and 3-hydroxysalicylic acid (H_2-3-hSA, 7.4 mg, 0.048 mmol) was dissolved in 10 mL of a DMF/EtOH/H_2O (15 : 1 : 1, v/v/v) mixed solvent. The solution was transferred to a 20 mL vial, tightly sealed and heated at 100 °C for 24 hours, resulting in **3-hSA$_{0.06}$**. The precipitate was collected, then washed at least three times using DMF, followed by solvent exchange with MeOH for at least five times over 3 days. Similarly, **3-hSA$_{0.21}$** and **3-hSA$_{0.41}$** were synthesized using the mole ratio of H_4DOBDC : H_2-3-hSA at 7 : 3 and 5 : 5, respectively. The crystalline product kept stored in MeOH before use in the experiment.

2.2.3. $[Ni_2(DOBDC)_{1-x}(2\text{-}hNA)_x(OH)_{2x}(H_2O)_{2+x}]$ (2-hNA$_x$). A solid mixture of $Ni(NO_3)_2 \cdot 6H_2O$ (198 mg, 0.680 mmol), H_4DOBDC (85.6 mg, 0.432 mmol) and 2-hydroxynicotinic acid (H_2-2-hNA, 6.7 mg, 0.048 mmol) was dissolved in 10 mL of a DMF/EtOH/H_2O (15 : 1 : 1, v/v/v) mixed solvent. The solution was transferred to a 20 mL vial, tightly sealed and heated at 100 °C for 24 hours, resulting in **2-hNA$_{0.06}$**. The precipitate was collected, then washed at least three times using DMF, followed by solvent exchange with MeOH for at least five times over 3 days. **2-hNA$_{0.17}$**, and **2-hNA$_{0.29}$** were synthesized using the mole ratio of H_4DOBDC : H_2-2-hNA at 7 : 3 and 5 : 5, respectively. The crystalline product kept stored in MeOH before use in the experiment.

2.2.4. $[Ni_2(DOBDC)_{1-x}(5\text{-}hBImCA)_x(OH)_{2x}(H_2O)_{2+x}]$ (5-hBImCA$_x$). A solid mixture of $Ni(NO_3)_2 \cdot 6H_2O$ (198 mg, 0.680 mmol), H_4DOBDC (85.6 mg, 0.432 mmol) and 5-hydroxy-1*H*-benzo[*d*]imidazole-4-carboxylic acid (H_2-5-hBImCA, 8.6 mg, 0.048 mmol) was dissolved in 10 mL of a DMF/EtOH/H_2O (15 : 1 : 1, v/v/v) mixed solvent. The solution was transferred to a 20 mL vial, tightly sealed and heated at 100 °C for 24 hours, resulting in **5-hBImCA$_{0.04}$**. **5-hBImCA$_{0.12}$** and **5-hBImCA$_{0.20}$** were synthesized using the mole ratio of H_4DOBDC : H_2-5-hBImCA at 7 : 3 and 5 : 5, respectively. The crystalline product kept stored in MeOH before use in the experiment.

3. Results and discussion

3.1. Synthesis and characterization of defect-engineered Ni-MOF-74 derivatives

To simultaneously achieve the defect generation and framework functionalization of the parent Ni-MOF-74, we selected H_2-5-fSA and H_2-3-hSA as defect-generating fragment organic ligands (Fig. 1). The 5-formylsalicylate (5-fSA)-incorporated defect-engineered Ni-MOF-74 derivative (denoted by **5-fSA$_x$**, where *x* represents the mole fraction of the integrated 5-fSA^{2-} at the $DOBDC^{4-}$ ligand sites of the framework) was synthesized by mixing H_4DOBDC with different molar ratios (from 10 to 50%) of H_2-5-fSA. The fragment installation was solvent-dependent: therefore, the defect-engineered MOFs could only be obtained in a DMF/EtOH/H_2O (15 : 1 : 1, v/v/v) solvent mixture.[15] The 3-

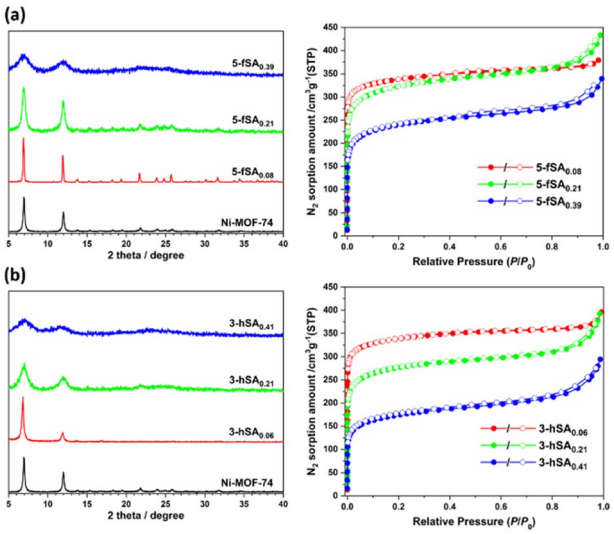

Fig. 2 PXRD patterns (left) and N_2 sorption isotherms (right) of (a) **5-fSA$_x$** and (b) **3-hSA$_x$**.

hydroxysalicylate (3-hSA)-incorporated derivative (**3-hSA$_x$**) was also prepared under the same synthetic conditions. The PXRD patterns of **5-fSA$_x$** and **3-hSA$_x$** showed that they were isostructural to the pristine Ni-MOF-74, and no other phase was present in the defect-engineered Ni-MOF-74 (Fig. 2). However, peak broadening was observed in the PXRD patterns at increasing mole fractions of 5-fSA^{2-} and 3-hSA^{2-}, indicating the low crystallinity of the defect-engineered MOF-74 at high feed ratios of the fragment (Fig. 2). The amount of fragment incorporated in the defective framework ranged from 8 to 39% for 5-fSA^{2-} and 6 to 41% for 3-hSA^{2-} (Fig. S1, S2 and Table S1, ESI†). Similar reactions were performed using two heteroaromatic fragments, H_2-2-hNA and H_2-5-hBImCA. Both fragments possessed –COOH and –OH groups on adjacent carbon atoms,

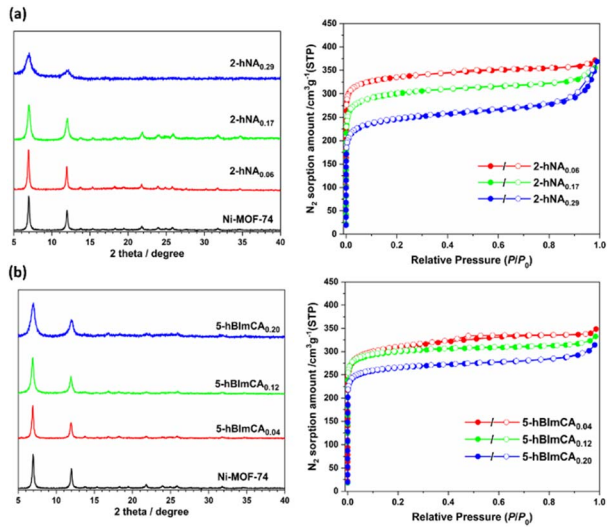

Fig. 3 PXRD patterns (left) and N_2 sorption isotherms (right) of the heteroaromatic fragment-incorporated defect-engineered Ni-MOF-74. (a) **2-hNA$_x$** and (b) **5-hBImCA$_x$**.

similar to those in salicylic acid (Fig. 1). The reactions resulted in finely powdered crystalline MOFs (**2-hNAx** and **5-hBImCA$_x$**) that were isostructural to the pristine Ni-MOF-74 (Fig. 3). When the initial feed ratio of H_4DOBDC : H_2-2-hNA or H_4-DOBDC : H_2-5-hBImCA was 50 : 50, the degree of fragment incorporation reached 20−30% (Fig. S3 and S4, ESI†). Remarkably, the defect-engineered MOFs exhibited thermal stability, comparable to that of pristine Ni-MOF-74 (Fig. S5, ESI†). They also showed excellent stability even in boiling water for 3 days. The PXRD patterns of defect-engineered MOFs recorded before and after exposure to boiling water did not show any significant broadening in the PXRD peaks, indicating that no deterioration of framework structure occurred in boiling water (Fig. S6, ESI†).

3.2. Porosity of defect-engineered Ni-MOF-74 derivatives

The introduction of fragmented ligands into the framework can affect the surface area and pore volume of defect-engineered MOFs.[18] To evaluate the effect of the fragmented ligand installation on the porosity of the MOFs, we measured their N_2 adsorption isotherms at 77 K. The activated defect-engineered Ni-MOF-74 exhibited type-I isotherms corresponding to microporous solids (Fig. 2 and 3). A continuous increase in N_2 adsorption was observed at high relative pressures ($P/P_0 > 0.80$) in all the defect-engineered Ni-MOF-74 derivatives with increasing defect concentration, suggesting that significant N_2 adsorption also occurred on the external surface of the MOFs.[19] This is because the external surface of the small sized (typically nanometer-sized) defect-engineered MOF derivatives is large enough to influence N_2 adsorption. The Brunauer–Emmett–Teller (BET) surface area of the defect-engineered MOFs ranged from 640 $m^2\ g^{-1}$ to 1325 $m^2\ g^{-1}$ with pore volumes of 0.456 $cm^3\ g^{-1}$ to 0.670 $cm^3\ g^{-1}$. As the incorporation level of fragmented ligands increased in the framework, the BET surface areas decreased (Table S2, ESI†). The BET surface area and pore volume of **5-fSA$_{0.08}$**, **5-fSA$_{0.21}$**, and **5-fSA$_{0.39}$** were 1325 $m^2\ g^{-1}$ and 0.586 $cm^3\ g^{-1}$, 1209 $m^2\ g^{-1}$ and 0.670 $cm^3\ g^{-1}$, and 894 $m^2\ g^{-1}$ and 0.517 $cm^3\ g^{-1}$, respectively. **3-hSA$_{0.06}$** had a BET surface area of 1323 $m^2\ g^{-1}$ and a pore volume of 0.608 $cm^3\ g^{-1}$, while the BET surface area of **3-hSA$_{0.21}$** (1042 $m^2\ g^{-1}$) was significantly reduced compared to **3-hSA$_{0.06}$**, the pore volume (0.607 $cm^3\ g^{-1}$) was almost the same. The further incorporation of 3-hSA^{2-} fragment led to the drastic decrease in porosity. **3-hSA$_{0.41}$** exhibited the most drastic decrease in porosity and the lowest surface area (640 $m^2\ g^{-1}$) and pore volume (0.456 $cm^3\ g^{-1}$) among the MOFs because of its poor crystallinity. For **2-hNA$_x$**, the BET surface area and pore volume of **2-hNA$_{0.06}$**, **2-hNA$_{0.17}$**, and **2-hNA$_{0.29}$** were 1325 $m^2\ g^{-1}$ and 0.575 $cm^3\ g^{-1}$, 1156 $m^2\ g^{-1}$ and 0.550 $cm^3\ g^{-1}$, and 934 $m^2\ g^{-1}$ and 0.570 $cm^3\ g^{-1}$, respectively. Similarly, the BET surface area and pore volume of **5-hBImCA$_{0.04}$**, **5-hBImCA$_{0.12}$**, and **5-hBImCA$_{0.20}$** were 1196 $m^2\ g^{-1}$ and 0.539 $cm^3\ g^{-1}$, 1189 $m^2\ g^{-1}$ and 0.514 $cm^3\ g^{-1}$, and 1038 $m^2\ g^{-1}$ and 0.486 $cm^3\ g^{-1}$, respectively. For **5-hBImCA$_x$**, the fragmented ligand 5-hBImCA^{2-} had the largest size, so a similar degree of incorporation resulted in the greatest reduction in surface area and pore volume.

The incorporation of fragmented ligands affected the pore size distributions of the defect-engineered MOF-74 derivatives. As the mole fractions of 5-fSA^{2-} increased, the pore-size distributions of **5-fSA$_x$** became wider while maintaining the same mean pore dimension (~12 Å) (Fig. S7, ESI†). A similar trend was observed for **3-hSA$_{0.06}$** and **3-hSA$_{0.21}$**, where **3-hSA$_{0.21}$** exhibited a broader distribution with the same mean pore dimension as **3-hSA$_{0.06}$** (~11 Å). However, further incorporation of 3-hSA^{2-} led to the drastically narrow pore size distribution with the mean pore dimension of 10 Å, as observed in **3-hSA$_{0.41}$**. In addition, pores with an extremely broad pore size distribution centered at ~20 Å with a total cumulative pore volume of 0.176 cm^3 g^{-1} were generated, corresponding to 40% of the total cumulative pore volume estimated up to 5 nm (Fig. S8, ESI†). This abnormal pore size distribution might have resulted from the low degree of crystallinity of **3-hSA$_{0.41}$** because of the simultaneous occurrence of fast crystal and defect formation in the presence of a large amount of H_2-3-hSA. For **2-hNA$_x$**, the mean pore dimension of 14 Å for **2-hNA$_{0.06}$** noticeably shifted to 12 Å for **2-hNA$_{0.17}$** and 10 Å for **2-hNA$_{0.29}$**. **5-hBImCA$_x$** exhibited a similar pore size distribution, with a mean pore diameter of 14 Å.

3.3. CO_2 adsorption of defect-engineered Ni-MOF-74 derivatives

The adsorption behavior of CO_2 can be affected by the functionalities of the MOFs.[20] To investigate the effects of functional groups on the CO_2 adsorption of defect-engineered Ni-MOF-74 frameworks, CO_2 adsorption isotherms were measured at 273 K (Fig. 4). The defect-engineered Ni-MOF-74 derivatives were grouped into three subgroups based on the incorporation level of fragmented ligands. At low incorporation levels (*i.e.*, ~10% or less than 10% of the incorporation level), **3-hSA$_{0.06}$** and **2-hNA$_{0.06}$** exhibited the highest CO_2 uptake (169–170 cm^3 g^{-1} at 1 bar and 273 K), followed by **5-fSA$_{0.08}$** (155 cm^3 g^{-1}) (Fig. 4a). **5-hBImCA$_{0.12}$** and **5-hBImCA$_{0.04}$** adsorbed 147 cm^3 g^{-1} and 139 cm^3 g^{-1} at 1 bar and 273 K, respectively. CO_2 adsorption isotherms were recorded at 195 K to calculate the maximal CO_2 uptake capacity (Fig. 4b).[21] **3-hSA$_{0.06}$** and **2-hNA$_{0.06}$** exhibited the equivalent maximum CO_2 uptake (311 cm^3 g^{-1}) at 1 bar. However, in the low-pressure region, **2-hNA$_{0.06}$** adsorbed more CO_2 than **3-hSA$_{0.06}$**. In addition, **5-fSA$_{0.08}$** and **5-hBImCA$_{0.12}$** showed almost equivalent CO_2 adsorption behavior with a maximum CO_2 uptake of 285 cm^3 g^{-1} at 1 bar. Among the MOFs containing ~20% of functionalized fragments, **5-fSA$_{0.21}$** exhibited the highest CO_2 uptake (143 cm^3 g^{-1} at 1 bar and 273 K), followed by **2-hNA$_{0.17}$** (138 cm^3 g^{-1} at 1 bar and 273 K) and **5-hBImCA$_{0.20}$** (121 cm^3 g^{-1} at 1 bar and 273 K) (Fig. 4c). Additionally, **3-hSA$_{0.21}$** exhibited the lowest CO_2 uptake (114 cm^3 g^{-1} at 1 bar and 273 K) among the MOFs in this category, owing to its poor crystallinity. At an incorporation level of ~30% or more, the CO_2 uptake drastically decreased for the defect-engineered MOFs owing to poor crystallinity (Fig. 4d). Overall, the CO_2 uptake of the defect-engineered MOFs exhibited a better correlation with the surface area than with the pore volume (Fig. S9, ESI†). Interestingly, **5-fSA$_x$** and **3-hSA$_x$** showed different CO_2 adsorption behaviors. At low incorporation levels of fragments, **3-hSA$_{0.06}$** exhibited slightly better CO_2 uptake than **5-fSA$_{0.08}$**. In contrast, **3-hSA$_{0.21}$** and **3-hSA$_{0.41}$** adsorbed significantly less CO_2 than **5-fSA$_{0.21}$** and **5-fSA$_{0.39}$**, which is attributed to the poor crystallinity of **3-hSA$_x$** at the high incorporation level of 3-hSA^{2-}. This observation is reminiscent of the lower degree of crystallinity of **3-aSA$_x$** (3-aminosalicylate-incorporated Ni-MOF-74) than **5-aSA$_x$** (5-aminosalicylate-incorporated Ni-MOF-74) at similar fragmented ligand loading levels, as reported in our previous study.[15] The poor crystallinity of **3-hSA$_x$** may be due to increased steric hindrance upon incorporation of 3-hSA^{2-}. The –CHO group of **5-fSA$_x$** points to the channel without steric hindrance, whereas the –OH group of **3-hSA$_x$** may slightly bump into the framework, resulting in the reduced crystallinity of the MOF.

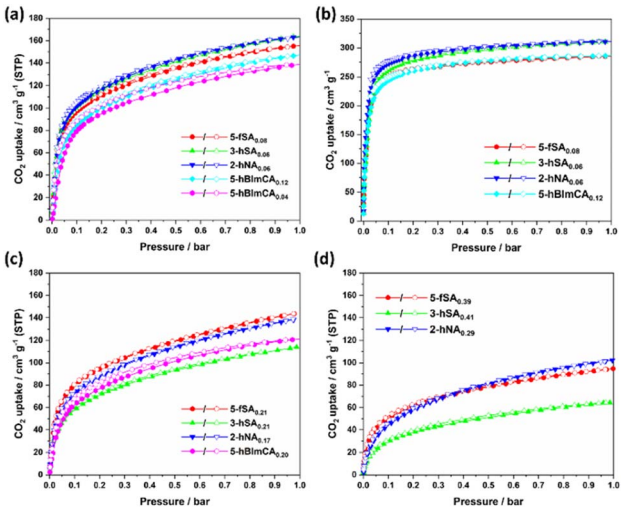

Fig. 4 CO_2 adsorption isotherms of functionalized defect-engineered Ni-MOF-74 derivatives grouped by the molar fraction of fragments (a) and (b) below 10%, (c) ~20%, and (d) exceeding 20%. (a), (c), and (d) were obtained at 273 K. (b) was obtained at 195 K.

3.4. Isosteric heat of adsorption for defect-engineered Ni-MOF-74 derivatives

The isosteric heat of adsorption (Q_{st}) is a critical factor in gas storage and adsorptive separation processes.[22] To estimate the Q_{st} values of defect-engineered Ni-MOF-74 derivatives, CO_2 isotherms of **5-fSA$_{0.08}$**, **3-hSA$_{0.06}$**, **2-hNA$_{0.06}$**, **5-hBImCA$_{0.12}$**, and defect-free Ni-MOF-74 were collected at 273 K, 283 K, and 293 K, respectively, and Q_{st} values were estimated using the virial method (Fig. S10–S14, ESI†). The Q_{st} values of CO_2 adsorption for defect-engineered MOFs ranged from 31 to 38 kJ mol^{-1} at low CO_2 loadings, and decreased gradually with increasing CO_2 uptake (Fig. 5). These Q_{st} values were comparable to or lower than that of defect-free Ni-MOF-74. This finding indicated that the CO_2 adsorption on the defect-engineered MOFs primarily occurred at the open metal sites inside the channel, as in the defect-free Ni-MOF-74.[10,23] Interestingly, **3-hSA$_{0.06}$** had slightly higher loading-dependent Q_{st} values than those of defect-free Ni-MOF-74, suggesting that the free hydroxyl group of **3-**

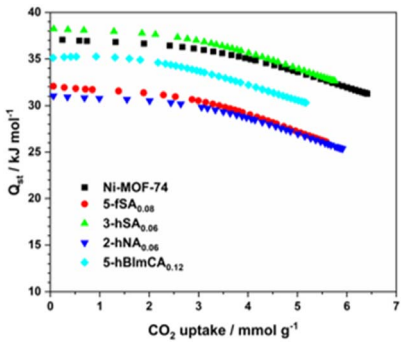

Fig. 5 Loading-dependent isosteric heats Q_{st} of CO_2 adsorption of functionalized defect-engineered Ni-MOF-74 derivatives.

hSA$_{0.06}$ also interacts with CO_2 molecule primarily bound to open Ni^{2+} ions inside the channel. A large CO_2 uptake capacity with a low Q_{st} value of the absorbent is important for the efficient regeneration of adsorbed CO_2 in an energy-saving adsorptive separation process. Lowering the Q_{st} values by incorporating fragmented ligands may provide insight into the development of adsorbents with high adsorptive separation potentials.

4. Conclusions

We synthesized a series of ligand-functionalized defect-engineered Ni-MOF-74 derivatives using a mixed-ligand synthesis approach. The crystallinity and microporosity of the functionalized defect-engineered MOFs depended on the mole fraction of the incorporated fragments and the type, position and size of the functional groups. The CO_2 uptake of defect-engineered MOFs strongly correlated surface area and crystallinity than with pore volume. At high incorporation levels, the functional groups and crystallinity became more important for the CO_2 uptake. The position of the functional groups and the size of the aromatic rings also affected the CO_2 uptake. Incorporation of fragmented ligands, except the fragmented ligand with –OH group, lowered the isosteric heat of CO_2 adsorption. Defect-engineered Ni-MOF-74 derivatives with high hydrothermal stability can be used for a variety of aqueous applications.

Conflicts of interest

There are no conflicts to declare.

Acknowledgements

This work was supported by grants (2016R1A5A1009405, 2022R1A2C2005339, and 2022R1I1A1A01071945) from the National Research Foundation (NRF) of Korea.

Notes and references

1 W. Xiang, Y. Zhang, Y. Chen, C.-J. Liu and X. Tu, *J. Mater. Chem. A*, 2020, **8**, 21526–21546.
2 S. Dissegna, K. Epp, W. R. Heinz, G. Kieslich and R. A. Fischer, *Adv. Mater.*, 2018, **30**, 1704501.
3 Z. Fang, B. Bueken, D. E. De Vos and R. A. Fischer, *Angew. Chem., Int. Ed.*, 2015, **54**, 7234–7254.
4 X. Hou, J. Wang, B. Mousavi, N. Klomkliang and S. Chaemchuen, *Dalton Trans.*, 2022, **51**, 8133–8159.
5 Z. Fan, J. Wang, W. Wang, S. Burger, Z. Wang, Y. Wang, C. Wöll, M. Cokoja and R. A. Fischer, *ACS Appl. Mater. Interfaces*, 2020, **12**, 37993–38002.
6 O. Kozachuk, I. Luz, F. X. Llabrés i Xamena, H. Noei, M. Kauer, H. B. Albada, E. D. Bloch, B. Marler, Y. Wang, M. Muhler and R. A. Fisher, *Angew. Chem., Int. Ed.*, 2014, **53**, 7058–7062.
7 Z. Fang, J. P. Dürholt, M. Kauer, W. Zhang, C. Lochenie, B. Jee, B. Albada, N. Metzler-Nolte, A. Pöppl, B. Weber, M. Muhler, Y. Wang, R. Schmid and R. A. Fischer, *J. Am. Chem. Soc.*, 2014, **136**, 9627–9636.
8 H. Deng, C. J. Doonan, H. Furukawa, R. B. Ferreira, J. Towne, C. B. Knobler, B. Wang and O. M. Yaghi, *Science*, 2010, **327**, 846–850.
9 J. H. Choe, H. Kim and C. S. Hong, *Mater. Chem. Front.*, 2021, **5**, 5172–5185.
10 W. L. Queen, M. R. Hudson, E. D. Bloch, J. A. Mason, M. I. Gonzalez, J. S. Lee, D. Gygi, J. D. Howe, K. Lee, T. A. Darwish, M. James, V. K. Peterson, S. J. Teat, B. Smit, J. B. Neaton, J. R. Long and C. M. Brown, *Chem. Sci.*, 2014, **5**, 4569–4581.
11 N. E. A. El-Gamel, *Eur. J. Inorg. Chem.*, 2015, 1351–1358.
12 D. Wu, W. Yan, H. Xu, E. Zhang and Q. Li, *Inorg. Chim. Acta*, 2017, **460**, 93–98.
13 J. A. Villajos, N. Jagorel, S. Reinsch and F. Emmerling, *Front. Mater.*, 2019, **6**, 230.
14 N. Heidary, D. Chartrand, A. Guiet and N. Kornienko, *Chem. Sci.*, 2021, **12**, 7324–7333.
15 J. Lim, S. Lee, H. Ha, J. Seong, S. Jeong, M. Kim, S. B. Baek and M. S. Lah, *Angew. Chem., Int. Ed.*, 2021, **60**, 9296–9300.
16 A. Koutsianos, E. Kazimierska, A. R. Barron, M. Taddei and E. Andreoli, *Dalton Trans.*, 2019, **48**, 3349–3359.
17 J. Park, Z. U. Wang, L.-B. Sun, Y.-P. Chen and H.-C. Zhou, *J. Am. Chem. Soc.*, 2012, **134**, 20110–20116.
18 G. Barin, V. Krungleviciute, O. Gutov, J. T. Hupp, T. Yildirim and O. M. Farha, *Inorg. Chem.*, 2014, **53**, 6914–6919.
19 T. Islamoglu, K. B. Idrees, F. A. Son, Z. Chen, S.-J. Lee, P. Li and O. K. Farha, *J. Mater. Chem. A*, 2022, **10**, 157–173.
20 Z. Hu, Y. Wang, B. B. Shah and D. Zhao, *Adv. Sustainable Syst.*, 2019, **3**, 1800080.
21 L. Liang, C. Liu, F. Jiang, Q. Chen, L. Zhang, H. Xue, H.-L. Jiang, J. Qian, D. Yuan and M. Hong, *Nat. Commun.*, 2017, **8**, 1233.
22 K. Sumida, D. L. Rogow, J. A. Mason, T. M. McDonald, E. D. Bloch, Z. R. Herm, T.-H. Bae and J. R. Long, *Chem. Rev.*, 2012, **112**, 724–781.
23 P. D. C. Dietzel, R. E. Johnsen, H. Fjellvåg, S. Bordiga, E. Groppo, S. Chavan and R. Blom, *Chem. Commun.*, 2008, 5125–5127.